19th Brazilian Congress of Thermal Sciences and Engineering
November 6th–10th, 2022, Bento Gonçalves - RS - Brazil

ENC-2022-0035
MODELING SINGLE JET DIFFUSION FLAME OSCILLATIONS BASED ON UNDER-SAMPLED DATA

Davi Saadi de Almeida Lettieri
Leonardo Santos de Brito Alves
Juan Carlos Assis da Silva
Departamento de Engenharia Mecânica, Universidade Federal Fluminense, Niterói, RJ 24210-240, Brasil
davilettieri@id.uff.br, lsbalves@id.uff.br, jcasilva@id.uff.br

Abstract. *Since first described, the Sparse Identification of Nonlinear Dynamics (SINDy) received significant attention from the scientific community as it represents one of the latest tools of symbolic regression in the machine learning field. Even though the original paper is relatively recent, there is already a large literature concerning its implementation and performance. However, most of it is focused on the rediscovery of a previously known dynamical system. Time-resolved images from an acoustic forcing experiment for the single jet diffusion flame oscillations are decomposed via Proper Orthogonal Decomposition (POD). After that, the most energetic modes with coherent structures are selected. However, the sampling rate of images was not enough to satisfy the Shannon Nyquist Theorem, and a spectral analysis alone is not sufficient to model the temporal behavior of each mode. On the other hand, the results indicate that looking at the 2D phase portraits can overturn the under-sampling problem.*

Keywords: *Machine Learning, Single Jet Diffusion Flame, SINDy, 2D Phase Portrait*

1. INTRODUCTION

1.1 Literature Review

We can observe combustion instabilities in almost all types of propulsion systems. Generally, they are understood as self-excited pressure oscillations in a combustion chamber product of an internal coupling between a perturbation and its driven mechanism. Moreover, they usually become a problem when we try to develop new systems looking for performance improvement. Unfortunately, the state of theory today does not provide a strong enough basis to predict combustion dynamics (Candel, 1992, 2002; Culick and Kuentzmann, 2006).

Recently, the Energy and Propulsion Research Laboratory at UCLA (University of California, Los Angeles) has been studying the flame dynamics produced by the combustion of individual droplets for different fuels under different external acoustic excitation (Bennewitz *et al.*, 2018; Karagozian, 2016; Sevilla-Esparza *et al.*, 2014). Here we highlight the work by Sim *et al.* (2020) which used the high-speed time-resolved images extending the analysis when extracted information via different types of modal decomposition. One of them was the Proper Orthogonal Decomposition (POD) which can be used to generate a nonlinear Reduced Order Model (ROM) capable of describing the behavior of the oscillatory flame (Candel, 2002).

The evolution of computer hardware and experimental apparatus brought an environment with plenty of data available for lots of different fields in science. It also encouraged the community to look for new developments in machine learning in general. Now fluid mechanics follows a trend of using data to easier extract valuable information (Brunton *et al.*, 2020). One of the most prominent methods was proposed by Brunton *et al.* (2016), the Sparse Identification of Nonlinear Dynamics (SINDy) promising a simple way to discover the governing equations of a nonlinear dynamics of interests using only data, taking advantage of sparse regression (Tibshirani, 1996) and compressed sensing (Donoho, 2006). It was a further step on many other works on symbolic regression (Bongard and Lipson, 2007; Schmidt and Lipson, 2009) which used genetic program (Koza, 1992). Since first published, SINDy has been used in different applications (Schaeffer, 2017; Narasingam and Kwon, 2018; Dam *et al.*, 2017) while others focused on the discussion among the major difficulties of implementation and new developments (Mangan *et al.*, 2016; Kaheman *et al.*, 2020).

A well-select model set has a big impact on the capability of SINDy to generate a ROM. Therefore, our work explores the difficulties when choosing the best models that describe the modes' temporal behavior with an under-sampled dataset.

It was observed that, on this task, the coefficient of determination along with the spectra analysis of fitted models are insufficient. On the other hand, the phase portraits seem to be an efficient way to at least rapidly discard models that at first glance seem in disagreement with the observed parametric curve shape.

1.2 SINDy

Therefore, the main objective of this paper is to show a new approach when one attempts to find the approximate functions that better fit the POD coefficients' temporal behavior. Hence, we separate this section to describe the SINDy and to indicate its necessity to use data with temporal precision. Since the long-term goal of our project is the development of ROM we may consider a system of ordinary differential equations in the general form

$$\frac{\partial \boldsymbol{\xi}(t)}{\partial t} = \boldsymbol{f}(\boldsymbol{\xi}(t)), \tag{1}$$

where the state vector and function can be written as

$$\boldsymbol{\xi}(t) = \{\xi_1(t), \xi_2(t), \ldots, \xi_n(t)\}^T, \tag{2}$$

and

$$\boldsymbol{f}(\boldsymbol{\xi}(t)) = \{f_1(\boldsymbol{\xi}(t)), f_2(\boldsymbol{\xi}(t)), \ldots, f_n(\boldsymbol{\xi}(t))\}^T. \tag{3}$$

Generally, a few assumptions must be made about Eq. (1), Eq. (2) and Eq. (3) to improve SINDy's performance. They are: (1) The state size n is arbitrary but small; (2) The state vector time history $\boldsymbol{\xi}(t)$ is available from data; (3) The state function $\boldsymbol{f}(\boldsymbol{\xi}(t))$ dependence on the state vector $\boldsymbol{\xi}(t)$ is unknown but sparse. In order to accomplish the second assumption, data is collected at a sampling rate m over a period $\tau = t_m - t_1$, then we build the matrices

$$\boldsymbol{\Xi} = \begin{pmatrix} \boldsymbol{\xi}(t_1)^T \\ \boldsymbol{\xi}(t_2)^T \\ \vdots \\ \boldsymbol{\xi}(t_m)^T \end{pmatrix} = \begin{pmatrix} \xi_1(t_1) & \xi_2(t_1) & \ldots & \xi_n(t_1) \\ \xi_1(t_2) & \xi_2(t_2) & \ldots & \xi_n(t_2) \\ \vdots & \vdots & \ddots & \vdots \\ \xi_1(t_m) & \xi_2(t_m) & \ldots & \xi_n(t_m) \end{pmatrix}_{m \times n} \tag{4}$$

and

$$\dot{\boldsymbol{\Xi}} = \begin{pmatrix} \dot{\boldsymbol{\xi}}(t_1)^T \\ \dot{\boldsymbol{\xi}}(t_2)^T \\ \vdots \\ \dot{\boldsymbol{\xi}}(t_m)^T \end{pmatrix} = \begin{pmatrix} \dot{\xi}_1(t_1) & \dot{\xi}_2(t_1) & \ldots & \dot{\xi}_n(t_1) \\ \dot{\xi}_1(t_2) & \dot{\xi}_2(t_2) & \ldots & \dot{\xi}_n(t_2) \\ \vdots & \vdots & \ddots & \vdots \\ \dot{\xi}_1(t_m) & \dot{\xi}_2(t_m) & \ldots & \dot{\xi}_n(t_m) \end{pmatrix}_{m \times n}, \tag{5}$$

where the last one is numerically approximated. After that, according to the third assumption we must define a library of candidate functions to estimate the unknown dependence of $\boldsymbol{f}(\boldsymbol{\xi}(t))$ on $\boldsymbol{\xi}(t)$. Hence, we propose the matrix

$$\boldsymbol{F}(\boldsymbol{\Xi}) = \begin{pmatrix} \vdots & \vdots & \vdots & \vdots & \vdots & \vdots \\ 1 & \boldsymbol{\Xi} & \boldsymbol{\Xi}^2 & \boldsymbol{\Xi}^3 & \ldots & \boldsymbol{\Xi}^p \\ \vdots & \vdots & \vdots & \vdots & \vdots & \vdots \end{pmatrix}_{m \times Q}, \tag{6}$$

where Q is the number of all different functions in the library and $\boldsymbol{\Xi}^p$ indicates the maximum nonlinearity order p^{th} for polynomial representation. For example, if $n = 2$ the submatrix $\boldsymbol{\Xi}^2$ contains every quadratic nonlinearities combinations between ξ_1 and ξ_2

$$\boldsymbol{\Xi}^2 = \begin{pmatrix} \xi_1^2(\boldsymbol{t}) & \xi_1(\boldsymbol{t})\xi_2(\boldsymbol{t}) & \xi_2^2(\boldsymbol{t}) \end{pmatrix}_{m \times 3}, \tag{7}$$

where t is the time vector. Moreover, it is important to notice that not necessary every element of ξ must have the same set of candidate functions. Actually, if any additional information about the system is known we should eliminate the maximum number of candidates possible. Finally, we define the matrix of unknown linear coefficients $\boldsymbol{\Gamma}$ as

$$\boldsymbol{\Gamma} = \begin{pmatrix} \gamma_{1,1} & \gamma_{1,2} & \cdots & \gamma_{1,n} \\ \gamma_{2,1} & \gamma_{2,2} & \cdots & \gamma_{2,n} \\ \vdots & \vdots & \ddots & \vdots \\ \gamma_{Q,1} & \gamma_{Q,2} & \cdots & \gamma_{Q,n} \end{pmatrix}_{Q \times n}, \tag{8}$$

where each element $\gamma_{i,j}$ represents the coefficient associated with the i^{th} candidate function for the j^{th} coordinate. Then, one can estimate the functional form of each $f_j(\boldsymbol{\xi}(t))$ from its respective data set $\boldsymbol{\Xi}_j$ by solving

$$\dot{\boldsymbol{\Xi}}_j^T = \boldsymbol{F} \cdot \boldsymbol{\Gamma}_j^T, \tag{9}$$

instead of Eq. (1) for each column $j = 1, 2, \ldots, n$.
It is important to note that $m \gg Q$ in most applications, i.e., $\boldsymbol{F}$ is a rectangular (low rank) matrix. Hence, Eq. (9) is over-determined and, in fact, represents a linear optimization problem. In order to take advantage of the third assumption, the objective function $\boldsymbol{v}_j$ to be minimized is usually defined as

$$\boldsymbol{v}_j = \|\dot{\boldsymbol{\Xi}}_j^T - \boldsymbol{F} \cdot \boldsymbol{\Gamma}_j^T\|_2, \tag{10}$$

where we use the standard SINDy algorithm with sequential thresholded least squares (STLQS), as the LASSO (Tibshirani, 1996) does not perform well at coefficient selection (Champion *et al.*, 2020). In this sense, we must define a vector parameter $\boldsymbol{\eta} = \{\eta_1, \eta_2, \ldots, \eta_n\}$, which works as cut parameter. For each equation of our system a linear regression is performed until convergence every time there is at least one coefficient with magnitude below the set parameter, dropping the candidate function associated with this coefficient.

2. RESULTS

The data used here represents only one set among other cases studied by Sim *et al.* (2020) where the flame dynamics of a single methane jet burning under acoustic forcing were investigated. The experimental apparatus consists of a cylinder working as a waveguide for the standing waves produced by two speakers assembled on both its extremes operating out of phase and has been detailed in other works (Sevilla-Esparza *et al.*, 2014; Bennewitz *et al.*, 2018). Those waves simulate an external acoustic excitation on the flame produced by the burner. The jet Reynolds number (Re) was set at 65 while the acoustic forcing frequency $f_a = 332\ Hz$. Moreover, the amplitude of the pressure perturbation, p'_{max} equals $100\ Pa$, characterizes the amplitude of acoustic excitation. For those parametric conditions, the flame behavior is described as sustained oscillatory combustion (SOC). Finally, a camera captured time-resolved visible images, at 1000 frames per second, which were then submitted to a Snapshot POD (Guan *et al.*, 2018) to extract information about the modes in the collected data.

In order to formulate a ROM for the flame oscillations dynamics, first we need to choose the modes that will be in our system of equations. The POD gives information on the most important structures present in a data set. Each one represents a dominant spatial behavior of the dynamics and are ordered based on the amount of relative energy it has. Looking at Fig. 1 we observe that the first five ones represent more than 97% of the cumulative energy and from the sixth onward we observe values same low magnitude. Furthermore, a similar behavior is indicated if we look at the maximum coefficient amplitudes for the same group. However, Fig. 3 shows that only the first four presents coherent structures while we can consider the further one are contaminated with noise.

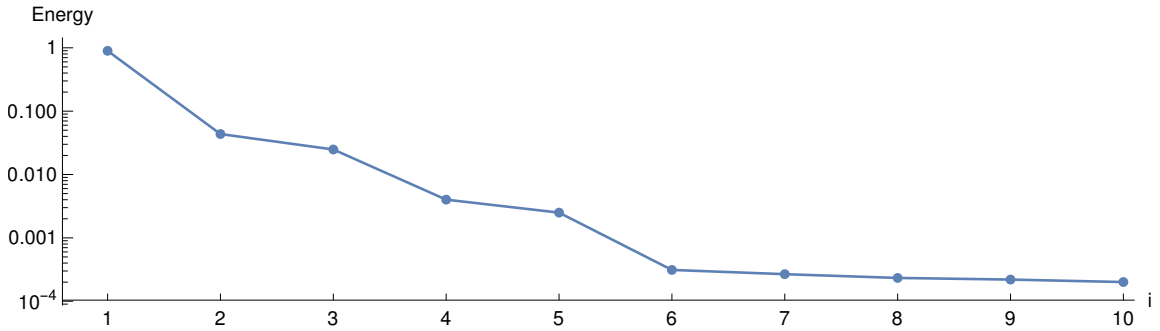

Figure 1: Relative energy of the first ten modes extracted from the POD.

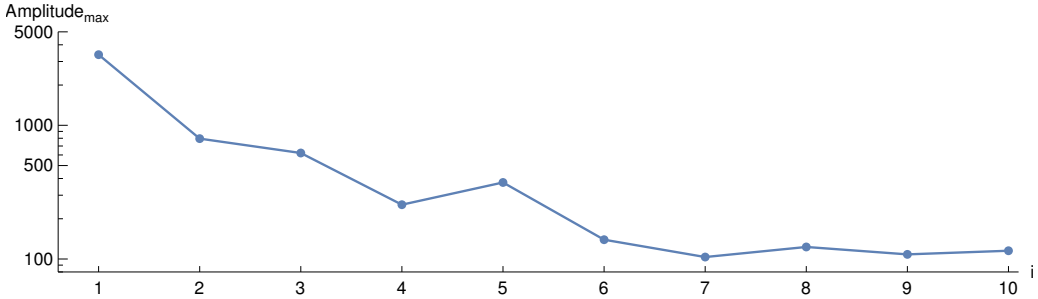

Figure 2: Maximum coefficient amplitude of the first ten modes extracted from the POD.

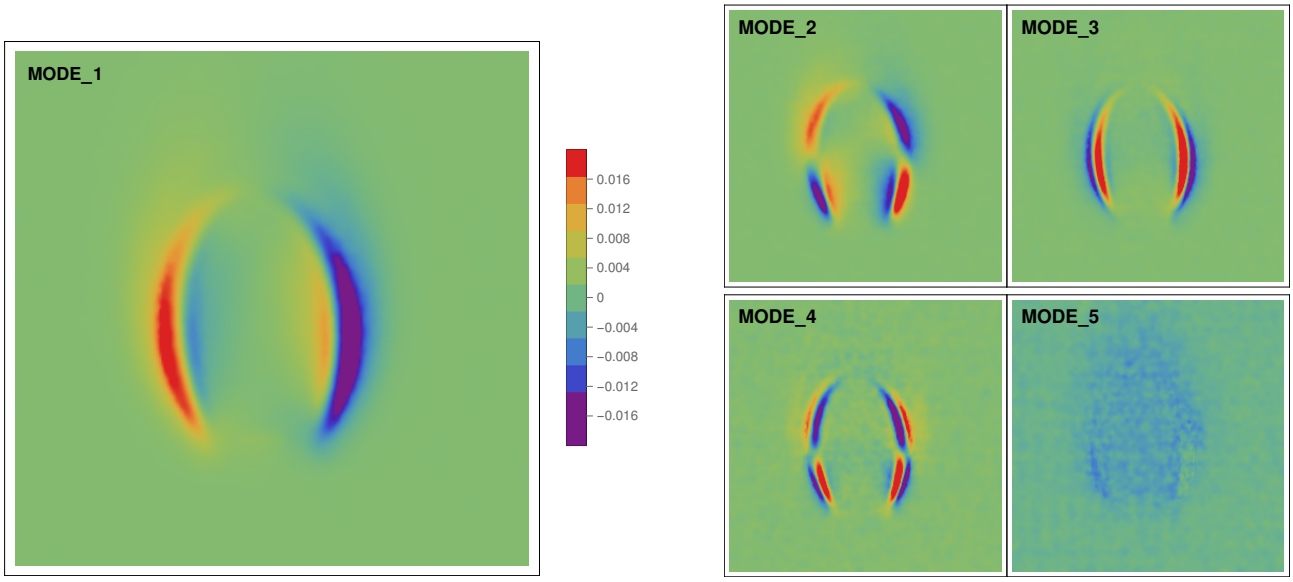

Figure 3: POD first five modes structures.

Furthermore, looking at the spectra information in Fig. 4 we can see that different from the previous four modes, which present a peak near the forcing frequency at 332 Hz indicating a coupling, the fifth one does not have a clear peak. That reinforce our assumption to discard the latter mode due to noise contamination.

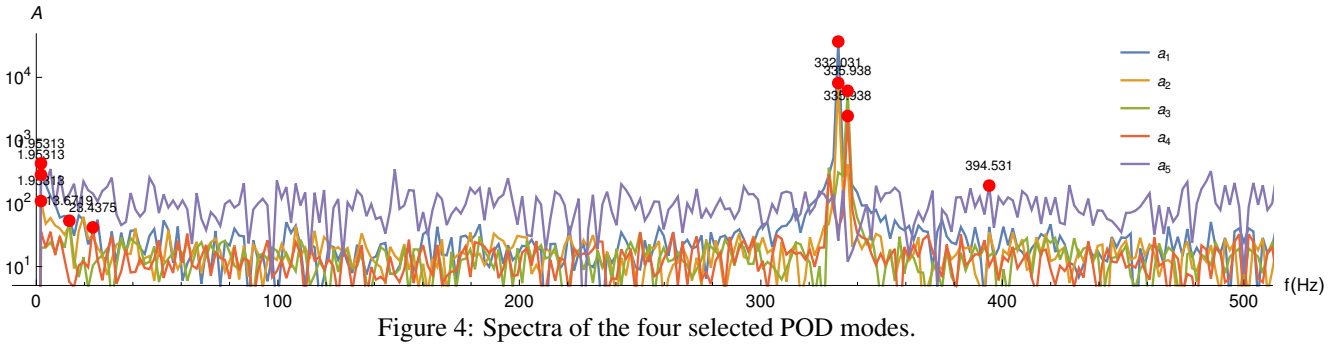

Figure 4: Spectra of the four selected POD modes.

In order to numerically construct the matrices $\dot{\boldsymbol{\Xi}}$ and $\boldsymbol{F}$ from Eq. 5 and Eq. 6, respectively, we must model the temporal behavior of each selected POD mode. Therefore, taking the following model structure

$$A\sin(2\pi Bt + C)^D + E\sin(2\pi Ft + G)^H \cos(2\pi It + J)^K + L\cos(2\pi Mt + N)^O, \tag{11}$$

where $A, B, C, D, E, F, G, H, I, J, K, L, M$ and N are the parameters. We fit the POD coefficients employing the initial guess of $332Hz$ for the frequency parameters. For each mode, several different models were tested, and we choose six of them. Their respective parameters corresponding to Eq. 11 are shown in Appendix. If we only compare their respective coefficient of determination R^2 we are not able to select any contender to discard, as Tab. 1 shows values with very close order of magnitude.

Table 1: Coefficient of determination (R^2) for the six models selected associated with each mode.

Mode	Model 1	Model 2	Model 3	Model 4	Model 5	Model 6
a_1	0.999918	0.999897	0.999783	0.999775	0.999775	0.999775
a_2	0.997056	0.996868	0.996626	0.996565	0.996490	0.996488
a_3	0.995489	0.995470	0.994981	0.994059	0.992631	0.989918
a_4	0.988583	0.979344	0.978651	0.977574	0.977144	0.976960

Almost in the same way, if we choose to look at their spectra, at least qualitatively, and compare it with the one generated by the original POD data, the differences we find are the number of peaks and its amplitude as Fig. 5 shows.

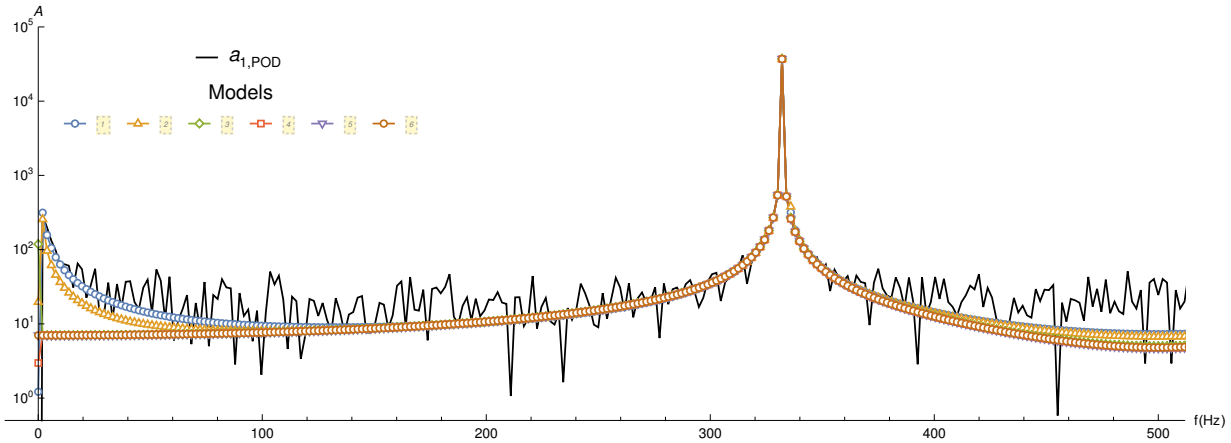

(a) Comparison between the spectra obtained from the POD data and the six selected models for a_1.

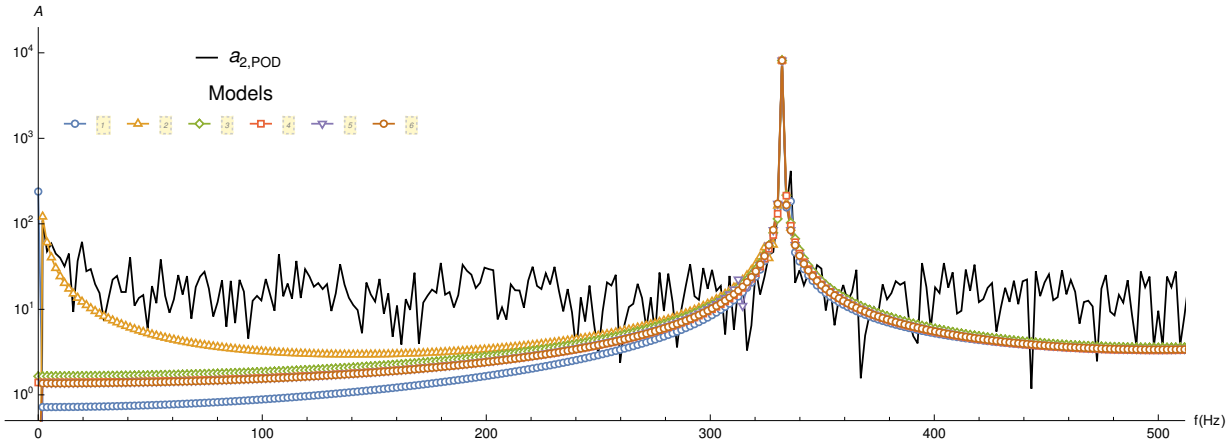

(b) Comparison between the spectra obtained from the POD data and the six selected models for a_2.

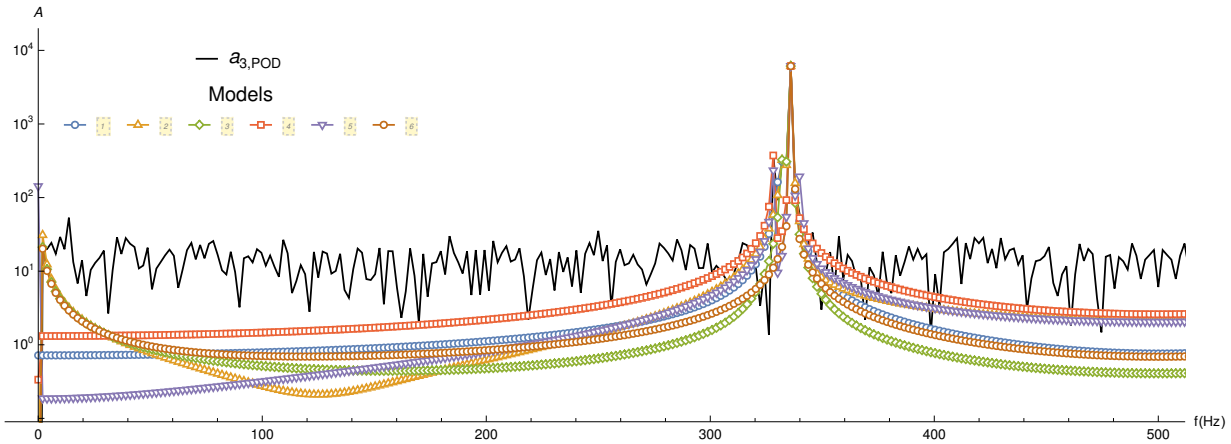

(c) Comparison between the spectra obtained from the POD data and the six selected models for a_3.

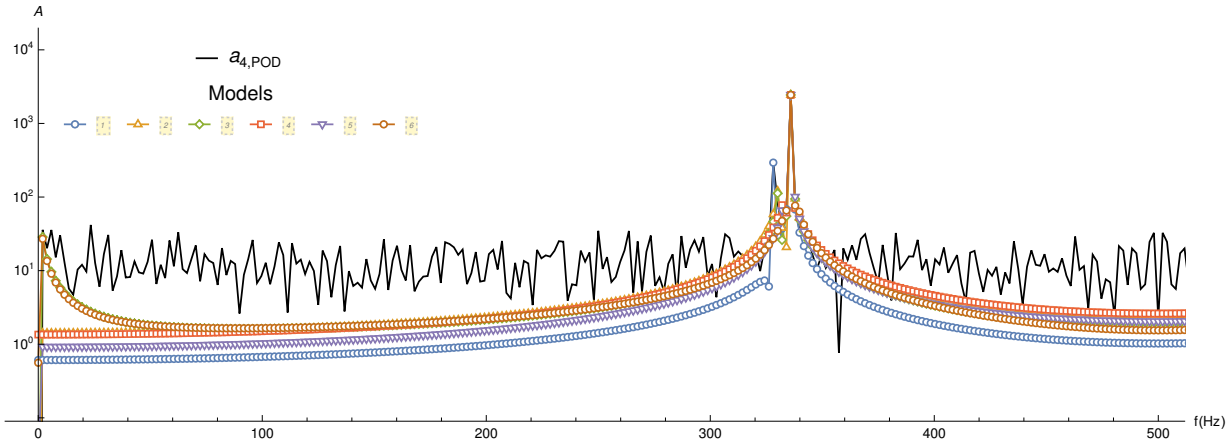

(a) Comparison between the spectra obtained from the POD data and the six selected models for a_4.

Figure 5: Comparison between the spectra obtained from the POD data and the six selected models for each mode.

Hence, in the same way, as for the coefficient of determination, there is no clear indication about which models we should discard. On the other hand, if we turn our attention to the 2D phase portraits between modes we can easily extract strong assumptions. Figure 6 represents an example of the latter when comparing the phase portraits between the POD data and the approximate functions derived from our models. Opposite to the trend mentioned before, when we set the sixth model as a_1 we observe a clear distinction if we choose the first or second model as approximations for a_2. While the topology of the first combination adjusts to the POD data trajectory over many periods, the second one does not.

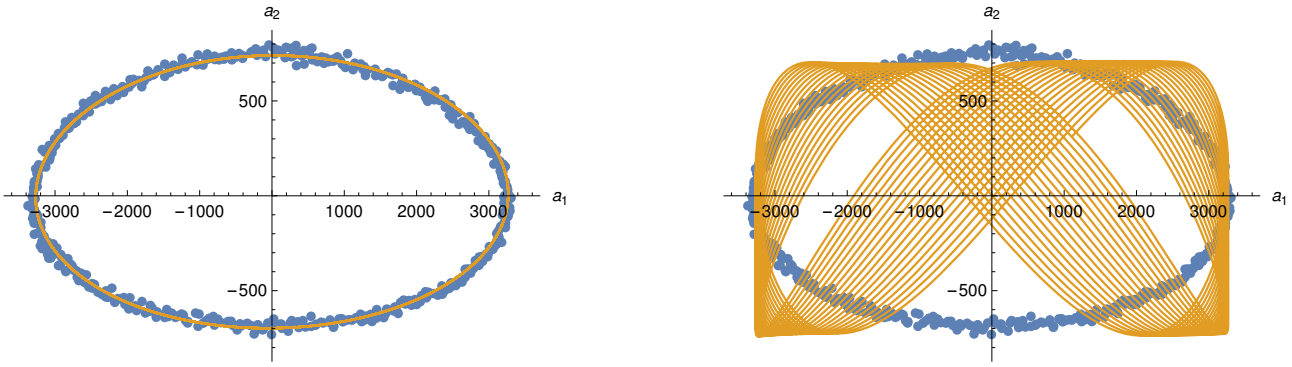

(a) a_1: Model 6 $\times$ a_2: Model 1

(b) a_1: Model 6 $\times$ a_2: Model 2

Figure 6: 2D Phase Portrait between the first and second mode obtained by the POD extracted data (blue points) and modeling of the temporal behavior for 20 periods (yellow line), where a period is equal to $1/332\ s \approx 3 \times 10^{-3}\ s$.

After that, a further analysis must be made among the combinations that reproduce an approximate behavior of the POD data in the 2D phase portraits. For this, we should look at aspects such as the number of periods within the trajectory remains on top of the closed topology or symmetries. Moreover, we can also use the nearest to 1 coefficient of determination and best fitted spectra as auxiliary for the best selection possible. Figure 7 shows all the comparison for every phase portrait for 100 periods when we choose the approximate functions as shown in Tab. 2.

Table 2: Model selected for each mode.

Mode	a_1	a_2	a_3	a_4
Model	6	1	3	3

From Fig. 7 we see that our selection captures the most important characteristics from the POD data one within a large number of periods. Thus it can be considered as the approximate functions that will build the matrix of derivatives to employ the SINDy and find a ROM.

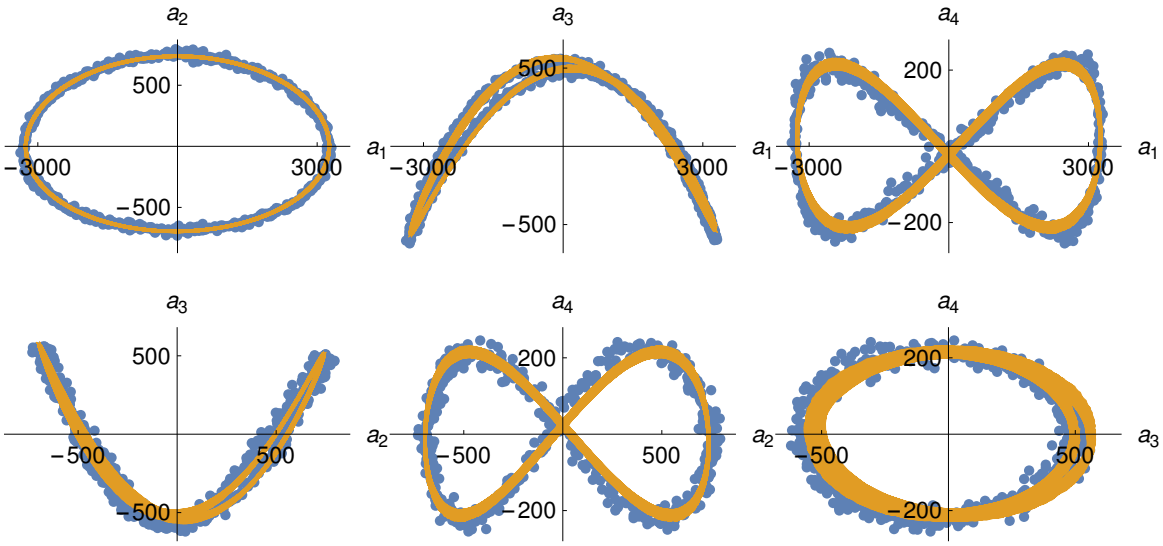

Figure 7: 2D Phase Portrait between each mode obtained by the POD extracted data (blue points) and modeling of the temporal behavior for 100 periods (yellow line).

3. CONCLUSION AND FUTURE WORKS

This work showed that the 2D phase portraits of the modes' coefficients represent an efficient method when choosing the best models that simulate its temporal behavior. While the coefficient of determination and the spectra can be used as auxiliary, they alone are insufficient when we need to make a selection. We look forward to exploring this criterion even more and extracting the maximum information possible from the topology to facilitate and improve the application of SINDy on POD data extracted from under-sampled time-resolved visible images.

4. ACKNOWLEDGEMENTS

The authors appreciate the financial support from CAPES.

5. REFERENCES

Bennewitz, J.W., Valentini, D., Plascencia, M.A., Vargas, A., Sim, H.S., Lopez, B., Smith, O.I. and Karagozian, A.R., 2018. "Periodic partial extinction in acoustically coupled fuel droplet combustion". *Combustion and flame*, Vol. 189, pp. 46–61.

Bongard, J. and Lipson, H., 2007. "Automated reverse engineering of nonlinear dynamical systems". *Proceedings of the National Academy of Sciences*, Vol. 104, No. 24, pp. 9943–9948.

Brunton, S.L., Noack, B.R. and Koumoutsakos, P., 2020. "Machine learning for fluid mechanics". *Annual Review of Fluid Mechanics*, Vol. 52, pp. 477–508.

Brunton, S.L., Proctor, J.L. and Kutz, J.N., 2016. "Discovering governing equations from data by sparse identification of nonlinear dynamical systems". *Proceedings of the national academy of sciences*, Vol. 113, No. 15, pp. 3932–3937.

Candel, S., 2002. "Combustion dynamics and control: progress and challenges". *Proceedings of the combustion institute*, Vol. 29, No. 1, pp. 1–28.

Candel, S.M., 1992. "Combustion instabilities coupled by pressure waves and their active control". In *Symposium (International) on Combustion*. Elsevier, Vol. 24, pp. 1277–1296.

Champion, K., Zheng, P., Aravkin, A.Y., Brunton, S.L. and Kutz, J.N., 2020. "A unified sparse optimization framework to learn parsimonious physics-informed models from data". *IEEE Access*, Vol. 8, pp. 169259–169271.

Culick, F. and Kuentzmann, P., 2006. "Unsteady motions in combustion chambers for propulsion systems". Technical report, NATO Research and Technology Organization Neuilly-Sur-Seine (France).

Dam, M., Brøns, M., Juul Rasmussen, J., Naulin, V. and Hesthaven, J.S., 2017. "Sparse identification of a predator-prey system from simulation data of a convection model". *Physics of Plasmas*, Vol. 24, No. 2, p. 022310.

Donoho, D.L., 2006. "Compressed sensing". *IEEE Transactions on information theory*, Vol. 52, No. 4, pp. 1289–1306.

Guan, Y., Murugesan, M. and Li, L.K., 2018. "Strange nonchaotic and chaotic attractors in a self-excited thermoacoustic oscillator subjected to external periodic forcing". *Chaos: An Interdisciplinary Journal of Nonlinear Science*, Vol. 28, No. 9, p. 093109.

Kaheman, K., Kutz, J.N. and Brunton, S.L., 2020. "Sindy-pi: a robust algorithm for parallel implicit sparse identification of nonlinear dynamics". *Proceedings of the Royal Society A*, Vol. 476, No. 2242, p. 20200279.

Karagozian, A.R., 2016. "Acoustically coupled combustion of liquid fuel droplets". *Applied Mechanics Reviews*, Vol. 68, No. 4.

Koza, J.R., 1992. *Genetic programming: on the programming of computers by means of natural selection*, Vol. 1. MIT press.

Mangan, N.M., Brunton, S.L., Proctor, J.L. and Kutz, J.N., 2016. "Inferring biological networks by sparse identification of nonlinear dynamics". *IEEE Transactions on Molecular, Biological and Multi-Scale Communications*, Vol. 2, No. 1, pp. 52–63.

Narasingam, A. and Kwon, J.S.I., 2018. "Data-driven identification of interpretable reduced-order models using sparse regression". *Computers & Chemical Engineering*, Vol. 119, pp. 101–111.

Schaeffer, H., 2017. "Learning partial differential equations via data discovery and sparse optimization". *Proceedings of the Royal Society A: Mathematical, Physical and Engineering Sciences*, Vol. 473, No. 2197, p. 20160446.

Schmidt, M. and Lipson, H., 2009. "Distilling free-form natural laws from experimental data". *science*, Vol. 324, No. 5923, pp. 81–85.

Sevilla-Esparza, C.I., Wegener, J.L., Teshome, S., Rodriguez, J.I., Smith, O.I. and Karagozian, A.R., 2014. "Droplet combustion in the presence of acoustic excitation". *Combustion and Flame*, Vol. 161, No. 6, pp. 1604–1619.

Sim, H.S., Vargas, A., Ahn, D.D. and Karagozian, A.R., 2020. "Laminar microjet diffusion flame response to transverse acoustic excitation". *Combustion Science and Technology*, Vol. 192, No. 7, pp. 1292–1319.

Tibshirani, R., 1996. "Regression shrinkage and selection via the lasso". *Journal of the Royal Statistical Society: Series B (Methodological)*, Vol. 58, No. 1, pp. 267–288.

6. RESPONSIBILITY NOTICE

The authors are solely responsible for the printed material included in this paper.

7. APPENDIX

Table 3: Coefficients associated with Eq. 11 of the selected models tested for mode 1.

Parameters	Model 1	Model 2	Model 3	Model 4	Model 5	Model 6
A	6535.93	3267.79	-	2347.15	476.473	3267.86
$B/2\pi$	2094.47	2081.96	-	2081.96	2081.95	2081.96
C	0.836601	3.03955	-	2.9115	2.49349	3.03909
D	2	1	-	1	1	1
E	6099.47	50.0761	3267.85	0.882803	-	-
$F/2\pi$	2081.2	2084.75	-	-	-	-
G	0.674889	0.219915	-	-	-	-
H	1	1	-	-	-	-
$I/2\pi$	2081.26	2077.96	-2081.96	2052.82	-	-
J	3.734	1.87627	4.81477	7.40775	-	-
K	1	1	1	2	-	-
L	-6119.83	-	11.0738	987.168	2872.28	-
$M/2\pi$	2081.23	-	2081.43	2081.97	2081.97	-
N	1.42076	-	2.89871	1.77569	1.55449	-
O	2	-	2	1	1	-

Table 4: Coefficients associated with Eq. 11 of the selected models tested for mode 2.

Parameters	Model 1	Model 2	Model 3	Model 4	Model 5	Model 6
A	-718.749	-468.631	-478.267	-436.976	1241.7	-1452.53
$B/2\pi$	-2081.91	-2049.75	-2079.69	-2083.36	2094.49	2094.49
C	4.80151	11.7559	3.12428	1.91914	5.23617	0.572739
D	1	1	1	1	2	2
E	-	1436.89	362.301	-	-1241.57	1452.67
$F/2\pi$	-	2094.56	-2078.92	-	2094.53	2094.53
G	-	0.814672	3.03591	-	5.84347	1.08229
H	-	1	1	-	2	2
$I/2\pi$	-	2094.47	-	-	-	-
J	-	0.837975	-	-	-	-
K	-	1	-	-	-	-
L	21.1442	-471.531	-706.334	1147.87	-0.921874	-
$M/2\pi$	2081.79	-2049.83	-2081.76	-2082.44	-1966.55	-
N	2.93897	13.3428	3.37575	0.183147	58.2275	-
O	2	1	1	1	1	-

Table 5: Coefficients associated with Eq. 11 of the selected models tested for mode 3.

Parameters	Model 1	Model 2	Model 3	Model 4	Model 5	Model 6
A	885.169	1037.55	-40.9338	-71.5152	32.3034	17.5551
$B/2\pi$	2080.82	-2081.83	2086.09	-2080.84	-2068.3	-2076.75
C	1.751	1.58802	0.522582	1.15777	0.089534	0.464847
D	1	2	1	2	2	2
E	-913.685	-534.384	-1069.93	574.047	542.974	1079.97
$F/2\pi$	2081.07	-2089.05	-2082	-	-	2082.09
G	1.69318	0.174462	2.41378	-	-	0.697318
H	1	1	1	-	-	1
$I/2\pi$	-	2089.78	-2082.02	2106.96	2106.78	2082.11
J	-	1.14771	2.41925	0.0813054	0.147839	0.708433
K	-	1	1	1	1	1
L	535.386	-507.3081	-	71.3694	-44.9288	-
$M/2\pi$	2106.97	2088.65	-	2107.43	2107.41	-
N	0.102968	6.17513	-	1.49751	6.23384	-
O	1	2	-	2	2	-

Table 6: Coefficients associated with Eq. 11 of the selected models tested for mode 4.

Parameters	Model 1	Model 2	Model 3	Model 4	Model 5	Model 6
A	215.663	436.991	-	678.246	380.459	598.564
$B/2\pi$	2106.97	2081.96	-	2104.76	2081.9	2079.95
C	0.100749	2.30779	-	0.733365	1.85866	2.88395
D	1	2	-	1	2	2
E	-	223.535	434.452	1019.73	-366.113	224.4
$F/2\pi$	-	-	2081.9	-	2081.92	2082.73
G	-	-	1.56287	-	1.23397	0.71423
H	-	-	1	-	2	1
$I/2\pi$	-	2080.05	2081.97	-2102.36	-	2083.06
J	-	2.55101	1.4957	3.29746	-	1.7897
K	-	1	1	1	-	1
L	-24.5798	-436.867	-21.1278	561.501	-14.2624	-393.001
$M/2\pi$	2057.27	-2095.26	-2097.83	-2089.94	-2079.3	-2079.3
N	7.72257	1.24214	0.162967	6.07525	0.178745	7.92175
O	1	2	2	1	2	2